Chiroptical properties of carbo[6]helicene derivatives bearing extended π-conjugated cyano substituents.

Mehdi El Sayed Moussa, Monika Srebro, Emmanuel Anger, Nicolas Vanthuyne, Christian Roussel, Christophe Lescop, Jochen Autschbach, Jeanne Crassous

Chiroptical properties of carbo[6]helicene derivatives bearing extended π-conjugated cyano substituents

MEHDI EL SAYED MOUSSA,[1] MONIKA SREBRO,[2] EMMANUEL ANGER,[1] NICOLAS VANTHUYNE,[3] CHRISTIAN ROUSSEL,[3] CHRISTOPHE LESCOP,[1] JOCHEN AUTSCHBACH,[4,*] JEANNE CRASSOUS[1,*]

[1] *Institut des Sciences Chimiques de Rennes, Campus de Beaulieu, UMR 6226 CNRS, Université de Rennes 1, 35042 Rennes Cedex, France*

[2] *Department of Theoretical Chemistry, Faculty of Chemistry, Jagiellonian University, 30-060 Krakow, Poland*

[3] *Aix-Marseille University, iSm2, CNRS, Chirosciences 13397 Marseille Cedex 20, France*

[4] *Department of Chemistry, University at Buffalo, State University of New York, Buffalo, NY 14260, USA*

*Correspondence to: Jeanne Crassous, Institut des Sciences Chimiques de Rennes, Campus de Beaulieu, UMR6226 CNRS - Université de Rennes 1, 35042 Rennes Cedex, France. E-mail: jeanne.crassous@univ-rennes1.fr. Jochen Autschbach, Department of Chemistry, University at Buffalo, State University of New York, Buffalo, NY 14260, USA, E-mail: jochena@buffalo.edu.

ABSTRACT New carbo[6]helicene derivatives grafted with π-conjugated cyano-phenyl arms have been synthesized in enantiopure forms and their π-conjugation examined by UV-vis spectroscopy. The influence of the π-conjugation on the circular dichroism spectra and molar rotations is discussed based on comparing experimental data with results from quantum chemical calculations. The results highlight the fact that increasing the π-system in a helicene molecule is an efficient way of increasing its molar rotation.

INTRODUCTION

Helicenes are ortho-fused nonplanar polyaromatic molecules with a unique helical shape combined with π-conjugation providing them with huge chiroptical properties (circular dichroism and optical rotation).[1-5] The development of chiral molecules revealing high chiroptical properties may lead to novel multifunctional molecular materials displaying chirality combined with other properties (circularly

polarized luminescence (CPL), optical or redox switching, gels or fibers formation, chiral recognition, etc...).[6] Helicene-based molecules may find applications in such domains, and attention has been recently paid on their properties.[7] Since the first synthesis and optical resolution of carbo[6]helicene in the mid-50s,[8] a number of helicene homologues have been prepared using different synthetic methods.[1-6,9,10] Among the various strategies available, an effective general method to obtain enantiopure helicenes involves *i*) the photocyclization of stilbenic systems to produce racemic helicenes,[11,12] and *ii*) the enantiomeric resolution of racemic helicene samples by preparative HPLC with appropriate chiral stationary phases.[13] Consequently, this enables to record experimental circular dichroism (CD) spectra and molar rotation values (MR) of enantiomeric helicenes and to compare them to the calculated ones, in order to get more insight into the different factors influencing these chiroptical properties. The impact on the CD spectra and MR values, of such factors as the helical pitch, the number of aromatic rings, the incorporation of heteroatoms or metallic ions, the substitution with conjugated groups, the positive or negative induction effect, the assembly of two helicenes, has been experimentally and theoretically studied.[14-24]

We have recently demonstrated that the chiroptical properties of helicenes can be engineered by introducing lateral organometallic substituents.[25] This result has highlighted the very important role of substituents grafted on the helicene core but incorporated in the π-system in determining its chiroptical properties. In this paper, we show that simple organic lateral vinyl or ethynyl π-substituents can greatly modify the chiroptical properties. We describe the synthesis and the enantiomeric resolution of novel carbo[6]helicene derivatives **H2-H4** (Fig. 1) bearing π-conjugated cyano substituents and examine their chiroptical properties by comparing experimental data with results mainly from density functional theory (DFT) and time-dependent DFT (TDDFT) calculations of structural parameters, optical rotations, and CD spectra.

RESULTS AND DISCUSSION

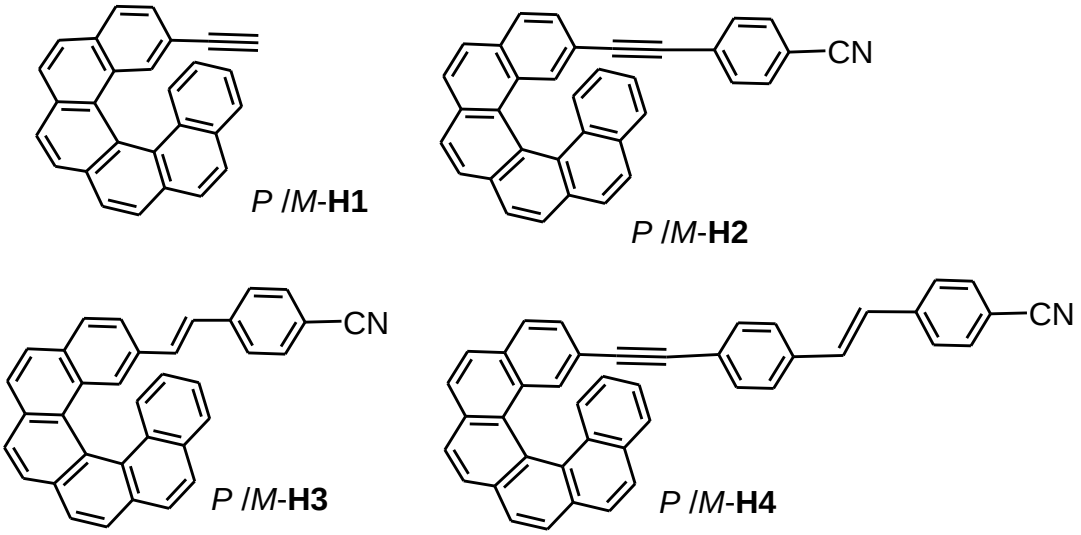

Fig. 1. Carbo[6]helicene derivatives **H1-H4**

A. EXPERIMENTAL RESULTS

A.1. Synthesis and resolution of helicene derivatives

Racemic **H2** was prepared from racemic 2-ethynyl-[6]carbohelicene **H1**[25] and the commercially available 4-bromobenzonitrile with 70% yield using classical Sonogashira coupling conditions (Scheme 1). Single crystals of racemic **H2** were grown by slow diffusion of pentane vapors into a CH_2Cl_2 solution and the X-ray crystallographic structure is depicted on Fig. 2 (P21/n space group). The overlapping of the terminal phenyl rings of the helicene moiety is clearly seen, with a helicity (dihedral angle between the terminal rings) of 48.5°, a classic value for a carbo[6]helicene derivative. Moreover, the coplanarity of the 4-cyano-phenyl-ethynyl moiety with the connected terminal phenyl ring of the helicene moiety is illustrated by the angle values of 173.6 and 177.4° for respectively C2-Ca-Cb and Ca-Cb-Cc and a dihedral angle of 15.2° between the benzonitrile and the phenylethynyl rings. This coplanarity ensures an efficient electronic coupling between the helicene core and the π-ligand and highlights the fact that **H2** is actually an extended π-conjugated helicene derivative. Enantiopure *P*- and *M*- **H3** were finally obtained by HPLC over Chiralpak IA (hexane/ethanol/chloroform (90/5/5) as the mobile phase). The experimental details are given in the SI part.

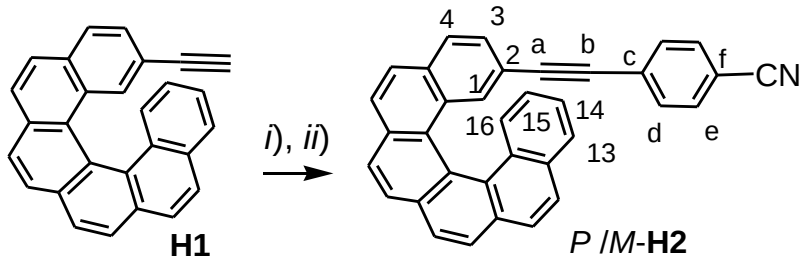

Scheme 1. Synthesis of enantiopure *P*- and *M*-**H2** from enantiopure *P*- and *M*-**H1**.[25] *i*) 4-bromobenzonitrile, $PdCl_2(PPh_3)_2$, CuI, Et_3N, Ar, 50°C, 1 night, 70%. *ii*) HPLC separation over a chiral stationary phase (*vide supra*).

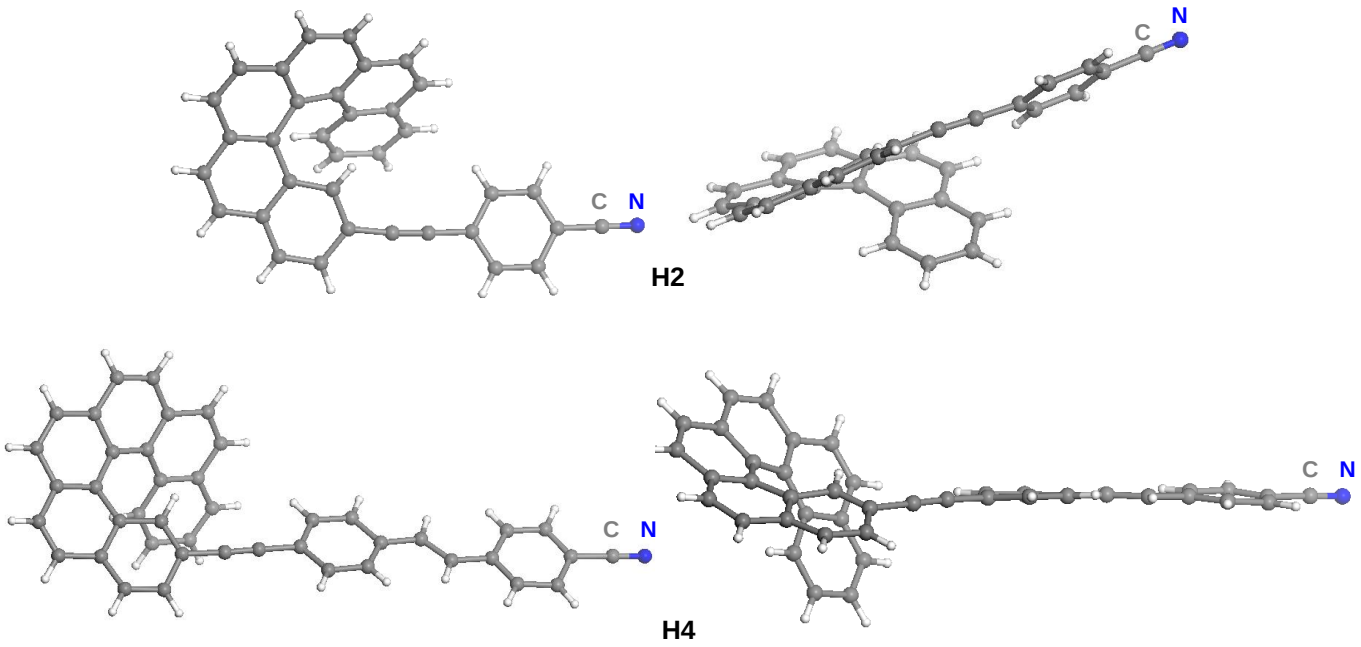

Fig. 2. X-ray crystallographic views of **H2** and **H4** (only the *P* stereoisomers shown).

The synthesis of *P*- and *M*- enantiomers of 4-cyanophenyl-vinyl substituted carbo[6]helicene **H3** was achieved according to Scheme 2. The first step was a classical Wittig reaction between the previously described benzo[c]phenanthrylphosphonium bromide **1**,[26] and commercially available 4-cyano-benzaldehyde, the reaction leading to olefin **2** with 85% yield as a mixture of the two *cis* and *trans* isomers that do not need to be separated for the next photocyclization reaction, a common reaction in the helicene synthesis.[11,12] Using classical photocyclization conditions (highly diluted toluene solutions in the presence of catalytic iodine and irradiation for one night using a 150W Hg lamp), 2-cyano-carbo[6]helicene **H5** was obtained with 45% yield after purification over column chromatography. The cyano group was then reduced to an aldehyde using DIBAL-H in toluene at 30°C, giving

carbo[6]helicene-2-carbaldehyde **H6**[28] with 85% yield. The final step was a Horner-Emmons reaction between the produced aldehyde **H6** and an already prepared 4-cyanobenzylphosphonate[27], yielding the desired product **H3** as a 30:70 *cis*/*trans* isomeric mixture. HPLC separation over a Chiralpak IB column (hexane/EtOH 8:2 as the mobile phase, see SI) enabled to obtain the final enantiopure *P*- and *M*- **H3** in their pure *trans* form (Fig. S1).

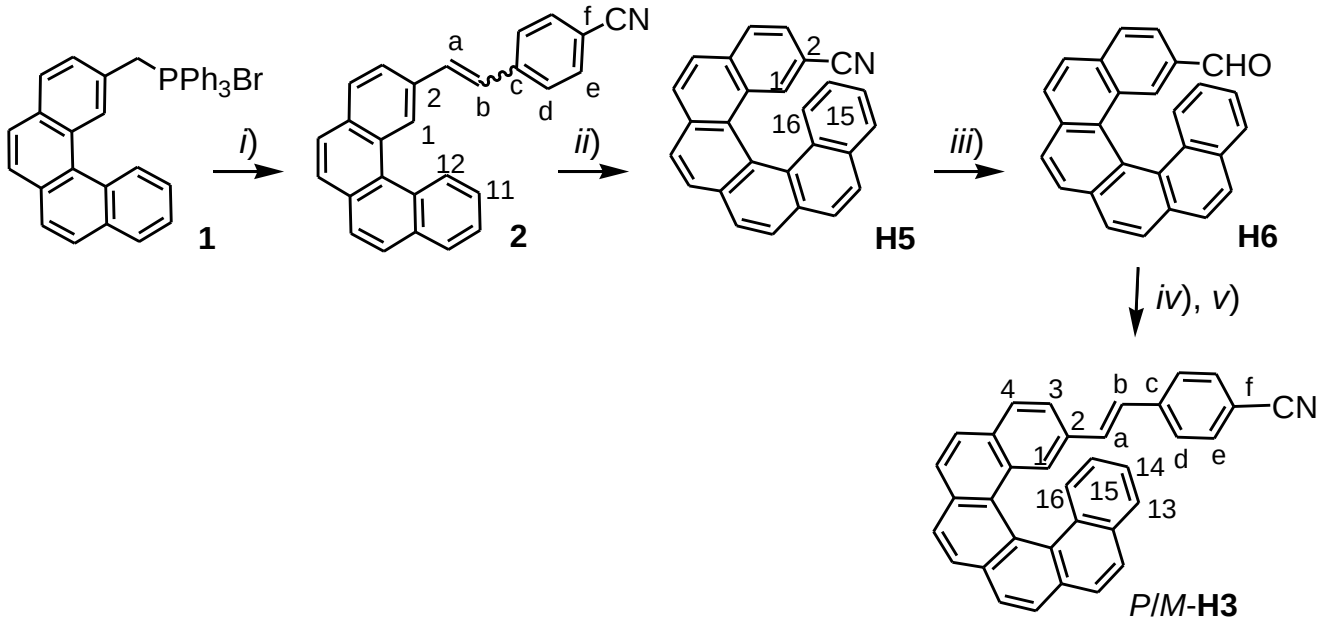

Scheme 2. Synthesis of enantiopure *P*- and *M*-**H3**. *i*) 4-cyano-benzaldehyde, *n*-BuLi, THF, Ar, r.t., 3 hrs, 85% ; *ii*) hν, cat. I_2, toluene, one night, 45%; *iii*) DIBAL-H, toluene, Ar, r.t., 2 hrs, 80%; *iv*) 4-cyanobenzylphosphonate[27], NaH, THF, Ar, 2 hrs, 80%; *v*) HPLC separation over a chiral stationary phase (*vide supra*).

The synthesis of *P*- and *M*- enantiomers of carbo[6]helicene **H4** substituted with a long π-conjugated arm was achieved according to Scheme 3. Racemic aldehyde **H7** was first prepared by a Sonogashira coupling between racemic **H1** and 4-iodobenzaldehyde with 92% yield. Then racemic **H4** was obtained by a Horner-Emmons reaction using 4-cyanobenzylphosphonate with 82% yield. Single crystals of racemic **H4** were grown by slow diffusion of pentane vapors into a CH_2Cl_2 solution and the X-ray crystallographic structure is depicted on Fig. 2. The structure was solved in the P-1 space group. The two phenyl rings of the stilbenyl moiety are almost coplanar with a dihedral angle of 6.5-7.6° between them. Moreover, the dihedral angle between the stilbenyl and the linked phenyl of the helicene core is between

28.8-30.6, values that still ensure efficient electronic coupling between the helicene core and the π-ligand. The carbo[6]helicene core displays a helicity (dihedral angle between the terminal rings) value of 49.6-50.4 °, which shows that the pendant π-system does not destabilize the helicene part. Here again, **H4** corresponds to an extended π-conjugated helical molecule. Finally, pure *P*- and *M*-**H4** enantiomers in their pure *trans* isomeric form were separated by HPLC over Chiralpak IC (Hexane/2-PrOH/chloroform (75/5/20) as the mobile phase, see SI).

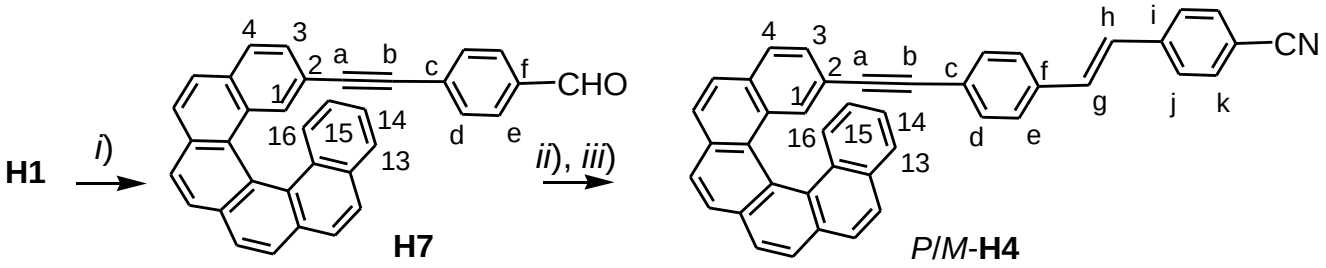

Scheme 3. Synthesis of enantiopure *P*- and *M*-**H4**. *i*) 4-iodobenzaldehyde, $PdCl_2(PPh_3)_2$, CuI, Et_3N, Ar, 50°C, 1 night, 92%; *ii*) 4-cyanobenzylphosphonate,[27] NaH, THF, Ar, 2 hrs, 82%; *iii*) HPLC separation over a chiral stationary phase (*vide supra*).

A.2. Experimental UV-Vis and chiroptical properties

In Fig. 3 are depicted the UV-vis spectra of helicene derivatives **H1**-**H4**. Ethynyl substituted **H1** displays several absorption bands below 380 nm (320, 332 and 352 nm) with moderate absorption coefficients (13000-26000 M^{-1} cm^{-1}). They are accompanied with two small bands at 390 and 410 nm. Compound 4-cyano-phenyl-vinyl substituted carbo[6]helicene **H3** displays broad absorption bands tailing down to 430 nm and more intense than in **H1** above 350 nm. Going from 4-cyano-phenyl-vinyl compound **H3** to 4-cyano-phenyl-ethynyl substituted **H2**, the absorption bands become much more intense (absorption coefficients up to twice as high as for **H3**) with several bands at 306, 329, 355, 395 and 417 nm, tailing down to 430-450 nm. In other words, phenyl-ethynyl substituted helicene **H2** is more conjugated than phenyl-vinyl substituted helicene **H3**, itself more conjugated than ethynyl-helicene **H1**, and increasing charge transfer is observed within the series **H1**→**H3**→**H2** (see also the discussion of the calculated CD spectra below). Finally, helicene **H4** substituted with 4-cyano-phenyl-vinyl-phenyl-ethynyle long arm displays an even more intense spectrum tailing down to ~450 nm, with bands at 334, 350, 359, 376, 400 and 417 nm, of intensities within the range 3700-50000 M^{-1} cm^{-1}. The UV-vis spectra therefore illustrate how the electronic properties of a carbo[6]helicene can be molecularly engineered by simply grafting a π-conjugated arm of different vinyl or ethynyl substituents and of different lengths. This simple method does therefore directly influence the chiroptical properties of helicenic systems.

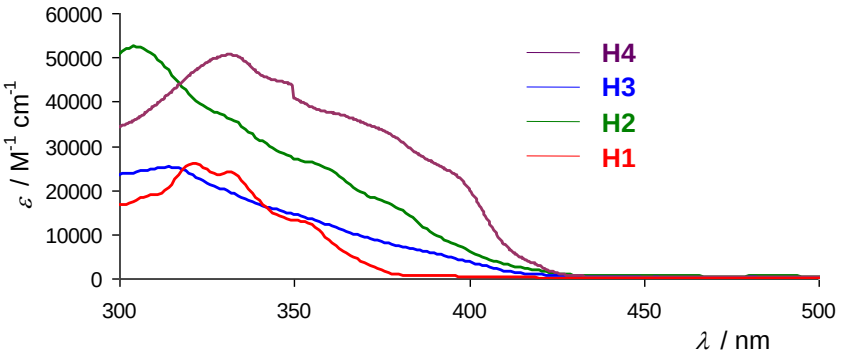

Fig. 3. UV-vis spectra of carbo[6]helicene derivatives **H1**-**H4**.

Fig. 4 displays the CD spectra of **H1**-**H4**. The *P* and *M* enantiomers reveal the expected mirror-image relationship. The experimental CD of *P*-**H1** and *P*-**H3** shows two intense CD bands at 250 nm (negative, ^1B_a transition according to the Platt nomenclature[29]) and around 335 nm (positive, ^1B_b transition) with a vibronic structure appearing. Note that the ^1L_b transition existing in helicene CD spectra is usually of very low intensity and not always seen and can change sign.[23,24] It is therefore difficult to identify. The CD shape of **H1**,**H3** corresponds to the common fingerprint of *P*-helicene derivatives. In Fig. 6 the CD spectra of the four *P*-**H1**-**H4** enantiomers are compared. As was already observed in UV-vis, the CD spectrum of **H3** is overall of lower intensity than **H1** with a slight bathochromic shift between 350-430 nm. The CD spectra of compounds **H2**,**H4** are sensibly different from **H1**,**H3** since they display two additional bands between 280 and 380 nm (negative, negative for *P*-**H2** and positive, negative for *P*-**H4**) beside the common intense negative bands at 250 nm and intense structured positive bands that appear highly bathochromically shifted (at 356 and 362 nm respectively). Very interestingly, Fig. 5 reveals that the ^1B_a transitions are of similar intensity in the four helicene derivatives. In contrast, the bands corresponding to the ^1B_b transition significantly change upon functionalization.[15,23,24,29]

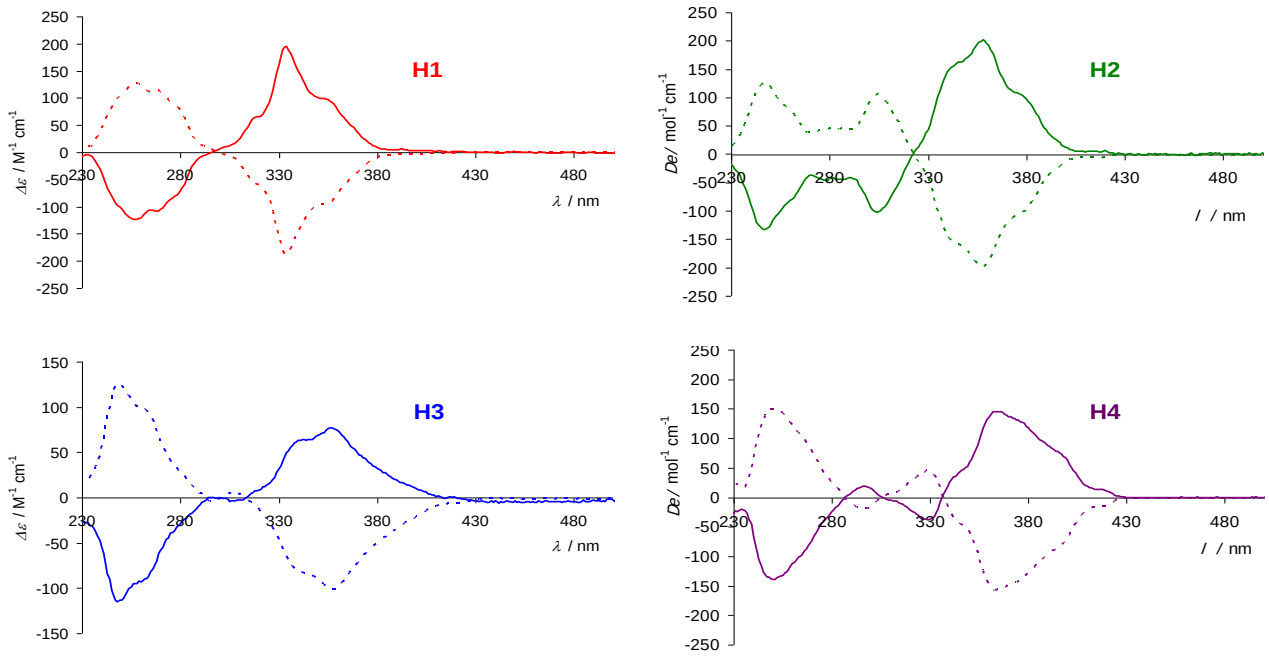

Fig. 4. CD spectra of enantiopure carbo[6]helicene derivatives **H1**-**H4**.

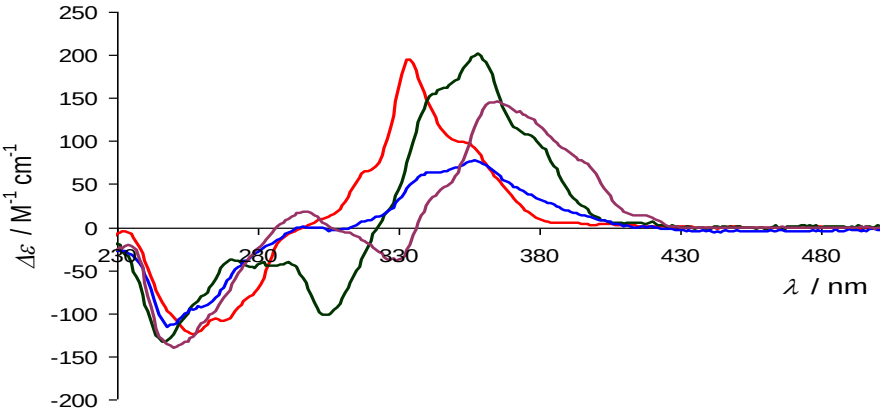

Fig. 5. CD spectra of **H1**-**H4** *P*-enantiomers.

The specific and molar rotations values are summarized in Table 1 (*vide infra*). The molar rotations display increasing values within the series **H3**<**H1**<**H2**<**H4**. They are clearly affected by the π-conjugation of the whole derivatives while the helicity of the helicene core is maintained. These results highlight the fact that increasing the π-system in a helicene molecule is an efficient way of increasing its molar rotation.

B. CALCULATIONS

B.1. Computational details

For compatibility with our previous work on helicene derivatives[18-22,25], DFT geometry optimizations were initially performed with the Turbomole program version 5.7.1[30,31], employing the BP[32-34] exchange-correlation functional and a split-valence basis set with one set of polarization functions for non-hydrogen atoms (SV(P))[35-37]. Computations with this functional and basis set combination are referred to as BP in the following. To provide further insight into the relationships between structure and chiroptical properties of the helicenes, subsequent geometry optimizations were performed with inclusion of dispersion (D) interactions. A subset of these calculations was carried out with the semi-empirical DFT-D3[38] approach as implemented in the Amsterdam Density Functional (ADF) program version 2012.01[39-41]. The DFT-D3 calculations employed the BP functional and an all-electron double-ξ (split valence) + polarization (DZP) Slater-type orbital basis for C and N along with a double-ξ (DZ) basis for H atoms. This set of calculations is referred to as BP-D in the following. An old branch of the optimization code in ADF 2012 was used after we found that the default, more recent, implementation of the optimizer produced nonphysical structures in conjunction with the D3 correction. Dispersion forces arise from dynamic fluctuating interactions between distant electrons due to electron correlation. Another subset of calculations employed Hartree-Fock (HF) theory followed by a perturbational treatment of electron correlation at the second-order Møller-Plesset level (MP2). The MP2 calculations were performed with the Gaussian 09 program[42], utilizing the correlation-consistent polarized double-ξ Dunning basis set cc-pVDZ[43] for all the atoms. For brevity, we refer to these calculations as MP2 in the following without explicitly indicating the basis set.

Time-dependent DFT (TDDFT) linear response calculations of optical rotation (OR) and circular dichroism (CD) were performed with NWChem 6.1[44,45] utilizing the optical activity module developed by one of the authors[46]. Optical rotation parameters were computed at the sodium *D*-line wavelength λ = 589.3 nm. The simulated CD spectra are based on calculations of the 60 lowest singlet vertical excitations and the corresponding electric and magnetic electronic transition dipole moments. The spectra were Gaussian broadened with a root mean square width parameter of σ = 0.2 eV.

The list of systems that were studied computationally includes the four carbo[6]helicene cyano derivatives **H1** – **H4** (Fig. 1) and, for comparison, the **H5** compound along with pristine [6]helicene. The latter is labeled as **H0** in order to indicate its role as the structural parent of **H1** – **H5**. For systems **H3** and **H4**, both s-*cis* and s-*trans* isomers as shown in Fig. 6 were considered. All calculations were carried out for the *P*-(+) isomers without imposing symmetry. The results for **H5** were found to be very similar to those for **H1**, which is not surprising because the two systems are isoelectronic. Furthermore, no detailed

experimental data are available for **H5**. Accordingly, **H5** is not discussed in detail. Results from a full set of calculations for **H5** can be found in the SI (Figures S10-S13, Tables S5 and S6).

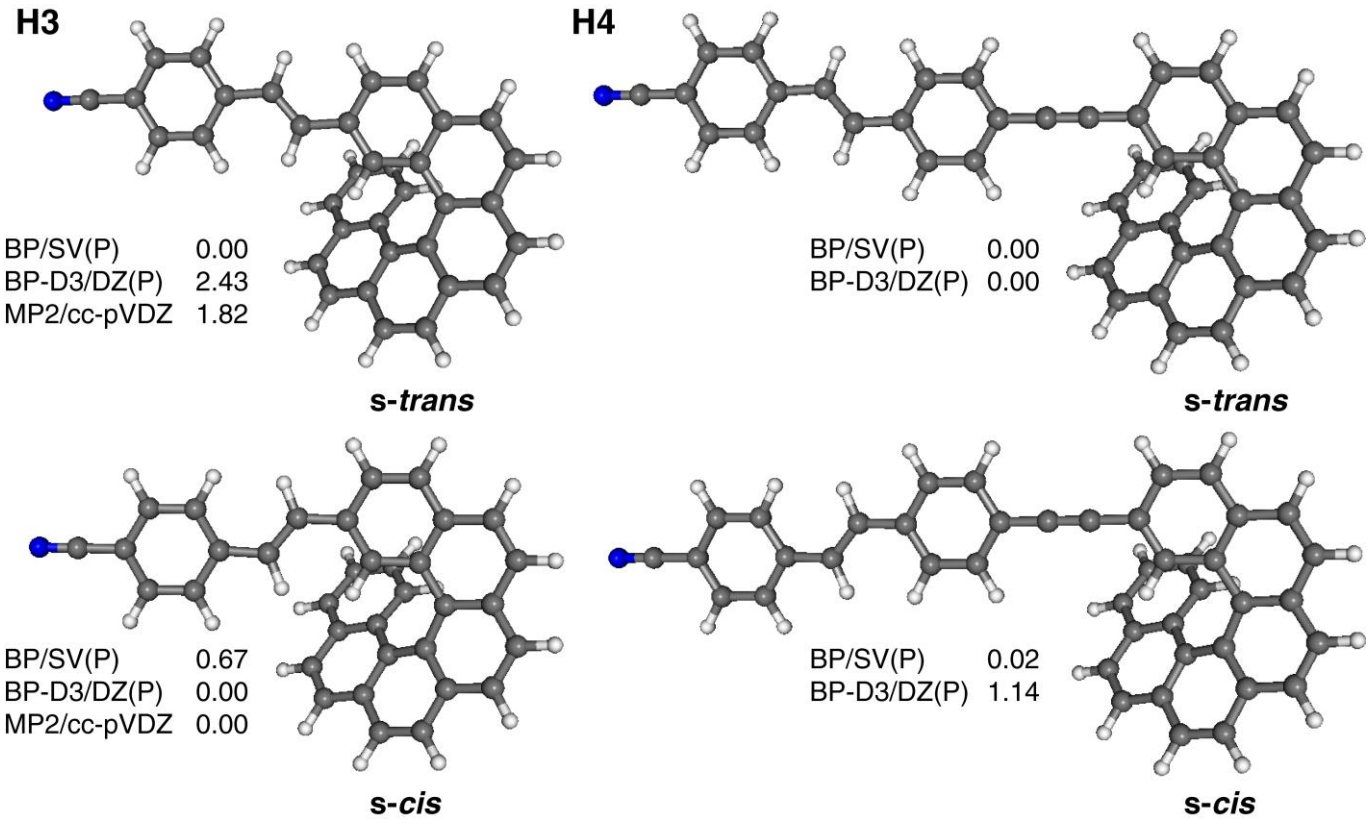

Fig. 6. Molecular structures of carbo[6]helicene derivatives **H3** and **H4**. Relative energies in kcal/mol are listed for the optimized BP/SV(P) (displayed), BP-D3/DZ(P), and MP2/cc-pVDZ geometries.

B.2. Benchmarks

In order to determine a computationally efficient, yet reliable, protocol for a description of the chiroptical properties of the samples, test calculations were initially carried out based on the BP geometries. For an overview of various influences that generally affect the computation of optical activity see Ref. 47. The main points addressed by the present calculations are (*i*) a possible origin dependence of the OR due to basis set incompleteness, (*ii*) the size of the basis set needed in order to obtain reasonable results for the helicene systems, (*iii*) the influence of approximations in the density functionals.

Regarding point (*i*), the standard length (L) representation of the electric transition dipole yields origin dependent isotropic chiroptical properties in calculations with finite AO basis sets. Although the

problem is associated with a gauge freedom for the magnetic dipole operator[48], the origin-dependence can be eliminated by adopting the velocity representation (V) of the electric dipole operator[49]. For OR, a modified velocity representation suggested in Ref. 50 was used. Alternatively, the origin-dependence is eliminated by adopting a distributed gauge origin for the magnetic vector potential, for instance by using a 'gauge-including' atomic orbital (GIAO) basis[46,51,52]. The three types of calculations (AO-L, AO-V, GIAO) become equivalent in the complete basis limit but they may generate very different results for finite basis sets. Since the AO-V and GIAO formalisms entail some additional computational cost, it was examined whether the computationally least demanding AO-L calculations are suitable for the helicene systems studied in this work (AO-V has additional overhead only for optical rotation, when using the 'modified' form). Regarding point (*ii*), it was examined whether diffuse basis functions are required for the present study. Results from computations with the aug-cc-pVDZ[43,53] basis *vs*. SV(P) were compared. Regarding point (*iii*), the list of examined functionals included two global hybrids, B3LYP[54-56] and BHLYP[55,57], and a hybrid functional with range-separated exchange and correct asymptotic potential, LC-PBE0[58-60] used in our previous benchmarks[14,61].

In line with helicene data from our recent 45-molecule OR benchmark (OR45[14]), the ORs show excellent agreement between the AO-L, AO-V, and GIAO calculations (Table S3). The agreement with experiment becomes better as the fraction of HF exchange in the functional increases, going from B3LYP to BHLYP to LC-PBE0 (Table S4 and Figure S2). Further, a substantial reduction in the basis set size when going from aug-cc-pVDZ to SV(P), does not change the MR values much (Table S4). This finding is in line with the rather good performance of SV(P) in many other studies on helicenes and helicene derivatives[18-22,25]. The underlying reason is that the OR is strongly dominated by valence excitations of low energy that barely have any contributions from hydrogen-centered AOs (see Section B.4). The CD over the UV-vis spectral range is assigned entirely to such valence transitions. Hence, computations of the OR and of the CD spectra in the UV-vis spectral range without diffuse basis functions and without polarization functions for hydrogen atoms are suitable for the purpose of this work. Accordingly, all subsequent computations employed the LC-PBE0 functional and the SV(P) basis set with AO-L gauge, using center of nuclear charges coordinates.

B.3. Geometry dependence of the optical rotations

Calculated molar rotations (MRs) $[\phi]_D$ for the helicene systems are listed in Table 1 along with available experimental data. Even though the LC-PBE0 functional gives ORs closer to experiment than the global hybrid functionals B3LYP and BHLYP (Table S4, Figure S2), except for **H0** the calculations

substantially overestimate the MRs for the BP optimized geometries (X = BP). Experimentally, only **H4** has a significantly larger OR than **H0**. Instead, **H1** and **H2** have ORs similar to **H0**, and the OR of **H3** is even lower. The overestimation of the calculated ORs with the BP geometries increases for systems with longer vinyl / ethynyl substituents, i.e. when going from **H1** to **H3** / **H4**. In fact, such a trend is *expected*. The π orbitals of the substituted systems exhibit pronounced π-conjugation between the helicene and the substituents, meaning that the effective chromophore length increases (compare Fig. 11 *vide infra*). In agreement with previous studies of substituted helicenes[14,18,19,61], the increased spatial extension of the helicene chromophore relative to **H0** intensifies the CD and increases the magnitude of the OR even though the substituent is not chiral itself (other than through a chiral induction when it is bound to the helicene). There is also an important influence from charge-transfer (CT) in the substituted helicenes, as shown in Section B.4.

Table 1. Molar rotations (deg cm^2 dmol^{-1}) calculated for **H0** to **H4**, and comparison with experiment.[a] Experimental specific rotations (deg/[dm (g/cm^{-3})]).

System	$[\phi]_D^{calc}$ LC-PBE0/SV(P)//X			$[\phi]_D^{expt\ b}$	$[\alpha]_D^{expt\ b}$
X =	BP	BP-D	MP2		
H0	10448	9532.2	9583.6	11954[c]	3640[c]
H1	13966	12050	12508	11030	3133
H2	18833	14727	11727	11900	2623
H3 s-*cis*	21393	13886	14302	---[d]	---[d]
H3 s-*trans*	19640	14551	11877	10650	2350
H4 s-*cis*	20329	17958	---[e]	---[d]	---[d]
H4 s-*trans*	20476	15000	---[e]	15820	2846

[a] X indicates the theoretical level used for the geometry optimization. AO-L calculations. [b] Measured in CH_2Cl_2. Concentrations: 0.03 g/100 mL. Error of 5-10%. [c] From Ref. 62. Recently, a value of 12348 was reported in Ref. 24. [d] No experimental data available. [e] MP2 optimizations did not converge.

In our recent studies[14] a pronounced dependence of the optical rotations of pristine and substituted helicenes on their molecular structure was noted. It was found that inclusion of van der Waals (dispersive)

forces may play a crucial role in geometry optimizations to ensure an accurate description of ORs in such compounds especially for more complex systems with π-conjugated substituents. One may distinguish two types of effects on the geometry of our samples: first, dispersion decreases the pitch of the helicene moiety through attractive π-stacking-like interactions. This effect reduces the magnitude of the OR. For **H0**, the reduction is about 10%, with very similar results from the optimizations with BP-D and MP2. For pristine [*n*]helicenes with not too large *n* and simple derivatives thereof, the reduction of the OR magnitude is within the accuracy limits of the TDDFT calculations. We have shown previously that the influence of the exact exchange in the range-separated functional, and the system-dependence of the range-separation parameter, may be of higher importance especially for systems with higher *n* [61]. A second effect from the dispersion forces affects the substituted helicenes, by producing large reductions in the distances between the substituent and the terminal aryl ring at the opposite end of the helicene moiety. Structure overlays for two representative molecules are shown in Fig. 7. The impact of this structural change on the OR may take place, for instance, *via* coupling of excitations involving orbitals centered in the substituent and the helicene terminus, respectively. Potentially, breaking or reducing the π-conjugation between the helicene and the substituent due to a bending of the linker moiety, as seen for **H2** in Fig. 7, may also have a strong effect. In the substituted helicenes, the helical pitch is reduced in optimizations with dispersion similar to what is found for **H0**. A comparison of X-ray crystal structures of **H2** and **H4** **s-*trans*** with BP, BP-D, and MP2 optimized geometries can be found in the SI (Figure S9). The effects of dispersion corrections on experimental structural parameters follow the general trends discussed in Ref. 61, in particular as far as the helical pitch is considered.

The ORs listed in Table 1 show a significantly improved agreement with experimental data when going from BP to BP-D and MP2 geometries. The dispersion effect on the geometries uniformly reduces the ORs, in some cases dramatically, meaning that the effects from the pitch reduction and from the reduced distance between ligand and helicene terminus add up. As a result, the ORs of **H1** to **H3** calculated with the MP2 optimized structures emerge as similar to that of **H0**; the effect from the increased effective chromophore length is counterbalanced by the dispersion corrections to the geometry. Visual inspection of the orbitals of **H1** to **H4** that yield dominant contributions to the CD spectrum (*vide infra*) indicate that the geometry changes due to dispersion interaction alter the extent of π-conjugation between the helicene moiety and the substituents only slightly. This assessment is further corroborated by the fact that the appearance of the CD spectra (Section B.4) is qualitatively similar for the structures with and without dispersion corrections. The spectra for the MP2 structures are, however, significantly less intense, which goes hand in hand with the reduction of the OR. We tentatively ascribe part of the large effects of the geometry changes on the ORs of **H2** to **H4** to excitonic coupling effects, similar to what has

been found previously for helicene-metal complexes[18,19]. Since the interaction is strongly distance-dependent (as indicated by the comparison between BP and BP-D or MP2 structures), there are potentially significant vibrational corrections to the OR[63] which may further improve the agreement with experiment and produce the correct trend among **H1**, **H2**, and **H3**.

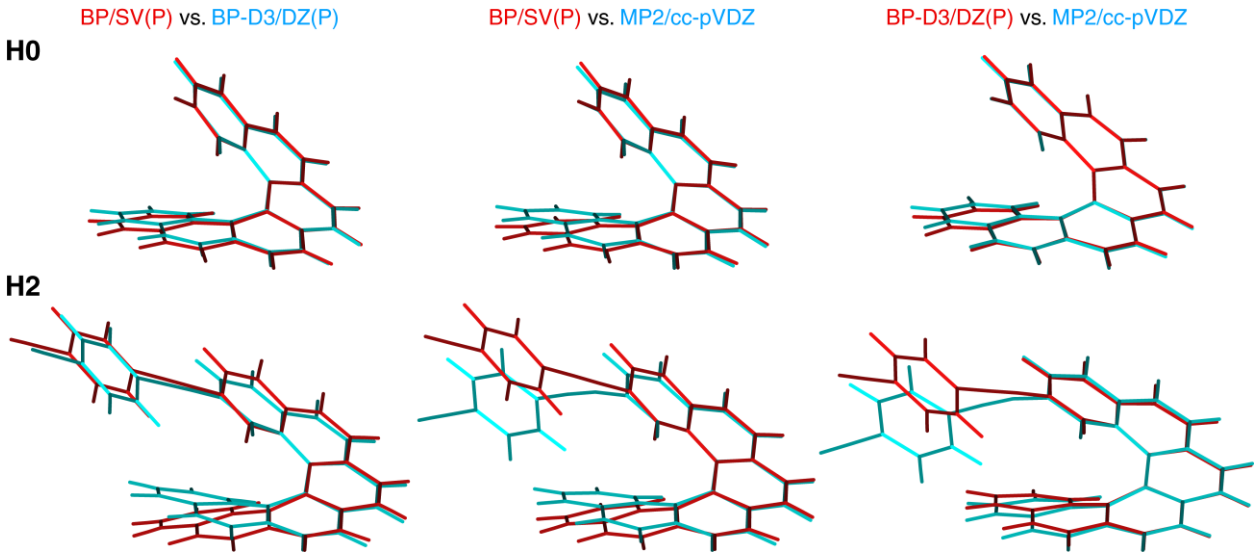

Fig. 7. Overlays of BP/SV(P), BP-D3/DZ(P), and MP2/cc-pVDZ optimized structures of **H0** and **H2**. See the SI for a complete set of overlay structures.

For the less complex systems **H0** and **H1**, the BP-D and MP2 geometries are very similar. Consequently, very similar ORs are obtained. Likewise, for **H3 s-*cis***, the geometries are quite similar, and so are the calculated ORs. **H3 s-*trans*** and **H2** show important differences between the BP-D and MP2 geometries. In the MP2 geometries, the substituent is closer to the helicene terminus, which amplifies the reduction of the OR discussed in the previous paragraph. In both cases, the calculated ORs with the MP2 structures are much closer to experiment than those obtained with the BP-D geometries (which already give a strong reduction relative to BP). The calculations further predict significantly larger ORs for the s-*cis* isomers of **H3** and **H4** than for the s-*trans* isomers, which would be interesting to confirm experimentally. Unfortunately, we were not able to converge MP2 geometry optimizations for **H4**. Irrespective of whether internal or Cartesian coordinates were optimized, large oscillatory forces on the atoms in the alkynyl linker persisted through many optimization steps. We attempted optimizations with another code and using additional approximations but obtained clearly deficient structures. Due to the rather high computational demand of the MP2 optimizations for **H4**, the approach was eventually abandoned and we decided to proceed only with the BP-D geometries. Fortunately, the calculated ORs agree well with experiment, which suggests that the optimized structure is reasonable. We speculate that a

structural distortion, similar to what is seen for **H2** when going from BP-D to MP2, would result in a too large energetic penalty from disrupting the pronounced π-conjugation between the helicene and the substituent which is visible, for instance, in the HOMO isosurfaces of **H4** (*vide infra*).

B.4. CD spectra

Fig. 8 displays comparisons of calculated and experimental spectra for each **H1**-**H4** system separately. To facilitate the interpretation of the theoretical results, Figures 9 and 10 compare the TDDFT UV-vis and CD spectra, respectively, for all systems in the same plot. A color scheme corresponding to the experimental data shown in Figures 3-5 is used here. Selected labeled excitations in the low-energy regions of the CD spectra (Fig. 10) have been characterized in detail. A list of pairs of occupied–unoccupied MOs that contribute with 10% weight or more to the transition density matrix of a selected excitation is provided in Table 2. The electric and magnetic transition dipoles are calculated from the transition density matrix, and therefore a large weight of a given pair of occupied and unoccupied MOs is indicative of their contributions to the intensity and provides an assignment of the excitation. Selected MOs are visualized in Fig. 11 (HOMOs and LUMOs) and Figures S4-S8.

Overall, the CD spectra agree well with experiment. The applied computational protocol typically does not yield intensities better than within a factor of 2 from experiment, and therefore the correct intensity ordering between **H2** and **H3** would be difficult to reproduce quantitatively. The main spectral features, and most importantly the sign patterns of the CD bands, are reproduced. The simulated spectra are based on Gaussian-broadened vertical excitations, and therefore they do not incorporate information on the vibronic structure of each CD band. As pointed out in the previous subsection, the spectra calculated with the MP2 geometries have lower intensity (in particular for **H2** and **H3**), which goes along with the significantly reduced ORs for these systems compared to the structures optimized without dispersion corrections.

H4 affords an intense positive CD band (from excitation no. 1) at particularly low energy, which is clearly a strong contributor to the large positive OR of this system. The MO analysis identifies this excitation as predominantly HOMO to LUMO. The relevant orbitals (Fig. 11) indicate that this transition affords π to π^* transition character in the substituent, as well as a pronounced degree of charge-transfer (helicene to substituent, and intra-substituent). The presence of CT character helps rationalizing the strong absorption intensity and low energy of the excitation. The enhancement of CT transition character due to the helicene π-electron system is nicely illustrated by a comparison of UV-vis spectra calculated for **H4** with two model systems – the pristine substituent HCCPhCHCHPhCN (**1**) and its phenyl

PhCCPhCHCHPhCN (**2**) derivatives (compare SI, Figures S14 and S15). Other notable excitations with strong CD are excitations no. 3 of **H0** and **H1**. The strong CD intensities results from the involvement of orbitals that extend over the full length of the helical chromophore (unlike excitation no. 1 in **H4** where only a small part of the helicene moiety is involved). Excitations no. 2 of **H2** and **H3**, with strong positive rotatory strengths and at lower energy than the intense transitions of **H0** and **H1**, are predominantly HOMO to LUMO and represent somewhat of a midpoint between **H0**/**H1** on the one hand and **H4** on the other: the excitations have helicene π to π^* character but only involve part of the helicene (reducing the CD intensity relative to the intense low-energy transitions in **H0** and **H1**), along with some clear helicene to ligand CT which is accompanied by an energy-lowering and a significant increase of the electric transition dipoles (boosting the intensities in the UV-Vis the absorption spectra). For **H4**, the electric transition dipole moment of excitation no. 1 is exceptionally strong due to the particularly pronounced CT character, as evident from the intense absorption spectrum in Fig. 9, while simultaneously involving part of the helicene chromophore. As a result, its rotatory strength is larger than those of excitations no. 2 of **H2** and **H3**. In summary, the spectra afford very clear systematic trends related to the presence and nature of the substituents, the extent of π-conjugation between the helicene moiety and the substituents, and the possibility of low-energy CT excitations that partially involve the helicene chromophore.

CONCLUSION

This case study of carbo[6]helicenes bearing extended π-conjugated cyano substituents nicely illustrates how the electronic and optical properties of an [6]helicene can be molecularly engineered by simply grafting a π-conjugated arm of different vinyl or ethynyl substituents and of different lengths therefore enabling to modify the chiroptical properties of helicenic systems. In the future, the ability of these phenyl-ethynyl and/or vinyl substituted carbo[6]helicenes bearing cyano groups to be used as ligands [27,64-67] for helicene-based coordination chemistry will be investigated.

Acknowledgments

This work has received financial support from the Centre National de la Recherche Scientifique (CNRS), the Ministère de l'Education Nationale, de la Recherche et de la Technologie, and the ANR program (12-BS07-0004-METALHEL-01) and the National Science Foundation (CHE 0952253). J.A. and M.S. thank the Center for Computational Research (CCR) at the University at Buffalo. M.S. acknowledges financial support from the Foundation for Polish Science ("START" stipend for young researchers).

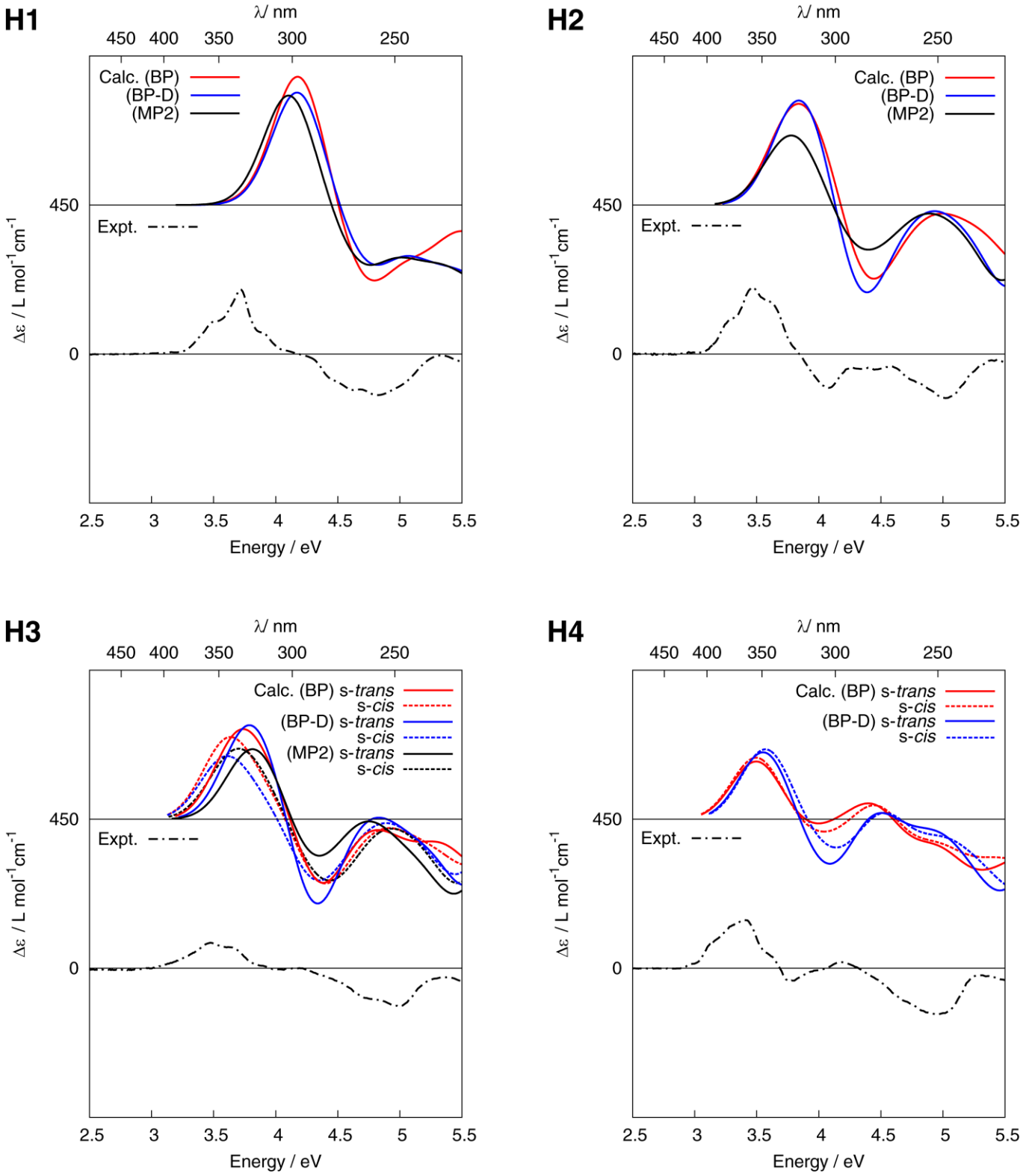

Fig. 8. Comparison of experimental and TDDFT LC-PBE0/SV(P) CD spectra of **H1**-**H4** *P*-(+)-enantiomers in their BP/SV(P) (BP), BP-D3/DZ(P) (BP-D), and MP2/cc-pVDZ (MP2) geometries. No spectral shift has been applied.

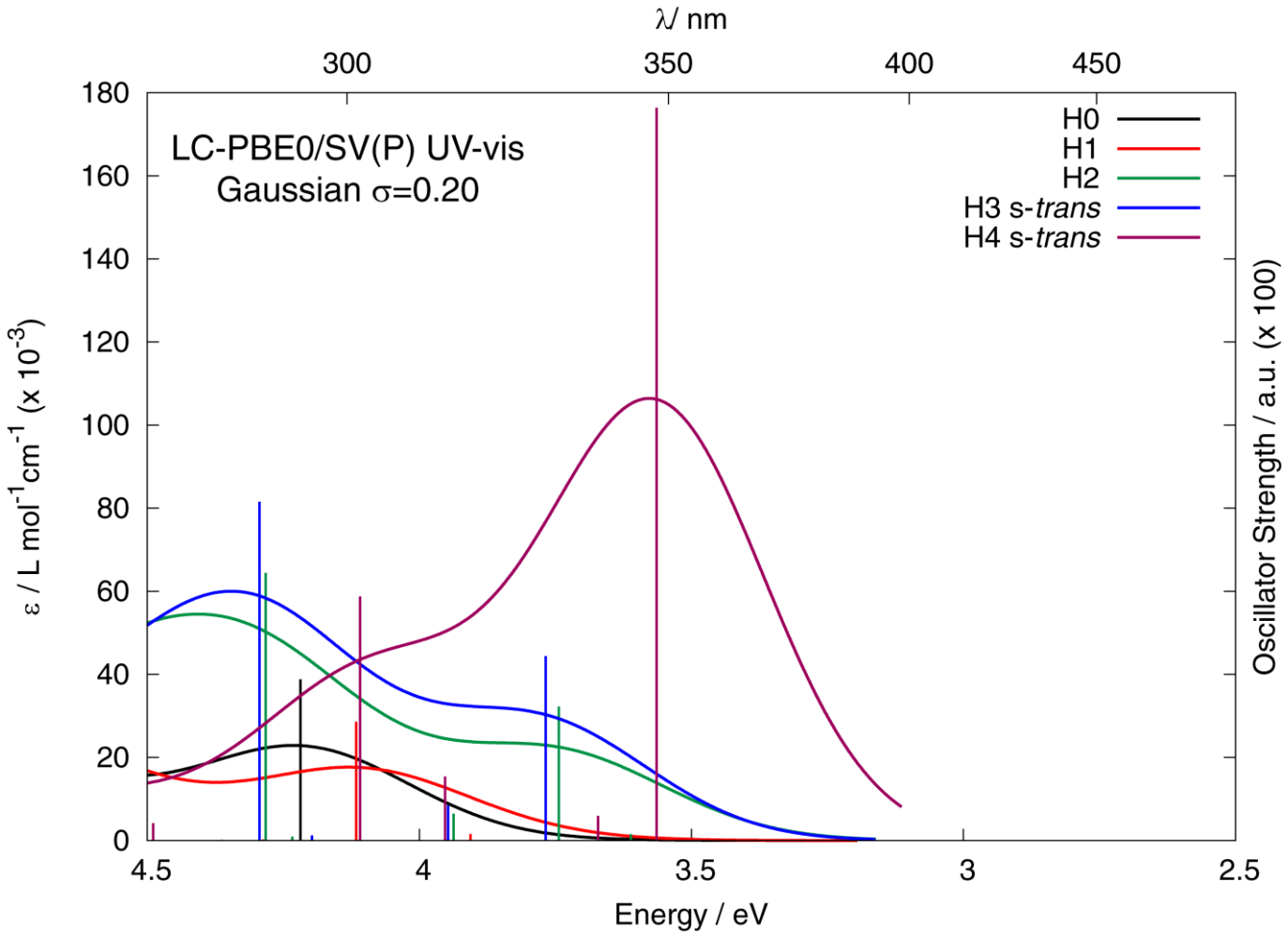

Fig. 9. Comparison of TDDFT LC-PBE0/SV(P) UV-vis spectra of *P*-**H0** (black line), *P*-**H1** (red), *P*-**H2** (green), *P*-**H3** **s-*trans*** (blue), and *P*-**H4** **s-*trans*** (purple). MP2/cc-pVDZ / BP-D3/DZ(P) geometries used for **H1**-**H3** / **H4**. No spectral shift has been applied.

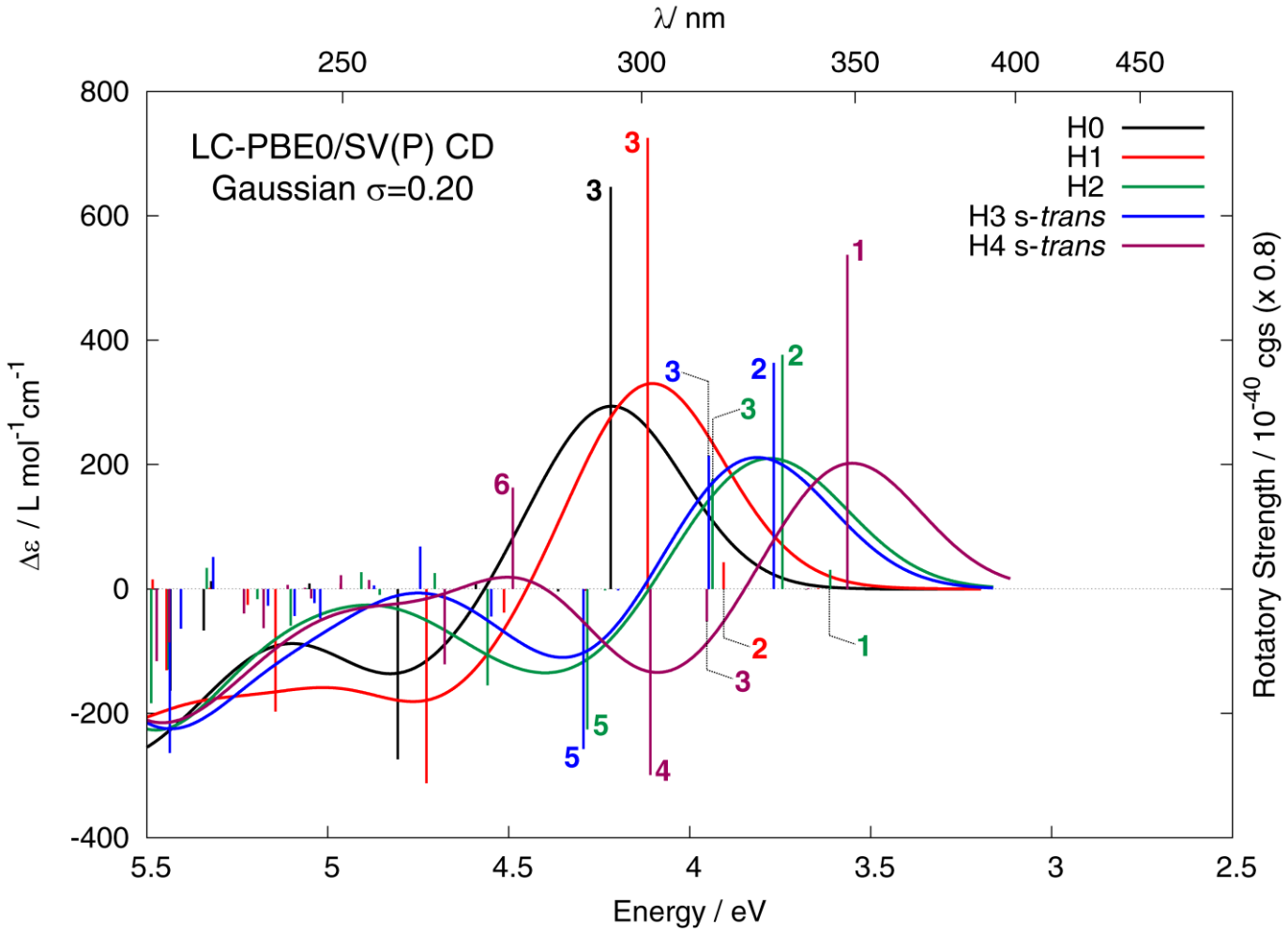

Fig. 10. Comparison of TDDFT LC-PBE0/SV(P) CD spectra of *P*-**H0** (black line), *P*-**H1** (red line), *P*-**H2** (green), *P*-**H3** **s-*trans*** (blue), and *P*-**H4** **s-*trans*** (purple). See also caption of Fig. 9. Numbered excitations correspond to those analyzed in Table 2.

Table 2. Dominant occupied (occ) – unoccupied (unocc) MO pair contributions (greater than 10%) of selected transitions of **H0**-**H4**, excitation energies *E* and rotatory strengths *R*. TDDFT LC-PBE0/SV(P) calculations for MP2/cc-pVDZ (**H0**-**H3**) and BP-D3/DZ(P) (**H4**) geometries.

Excitation	*E* / eV	*R* / 10^{-40} cgs	occ no.	unocc. no	%
			***P*-H0**		
#3	4.22	808.30	86	88	48
			85	87	36
			***P*-H1**		
#2	3.91	53.69	91	93	64
			92	94	24
#3	4.12	907.08	91	94	37
			92	93	27

			92	94	15
			***P*-H2**		
#1	3.61	38.34	118	120	30
			117	121	17
			118	119	14
#2	3.74	470.89	118	119	52
			117	119	17
			117	121	10
#3	3.94	220.67	117	120	58
			118	121	11
#5	4.28	-282.53	116	119	20
			117	121	19
			118	120	13
			117	119	10
			P*-H3 s-*trans		
#2	3.77	454.33	119	120	67
#3	3.95	267.99	118	121	63
#5	4.29	-321.68	118	120	16
			117	120	15
			118	122	14
			117	121	12
			119	121	11
			P*-H4 s-*trans		
#1	3.56	671.79	145	146	63
#3	3.95	-65.09	144	147	41
#4	4.11	-373.95	144	148	40
			145	147	17
			143	146	10
#6	4.49	203.70	142	147	27

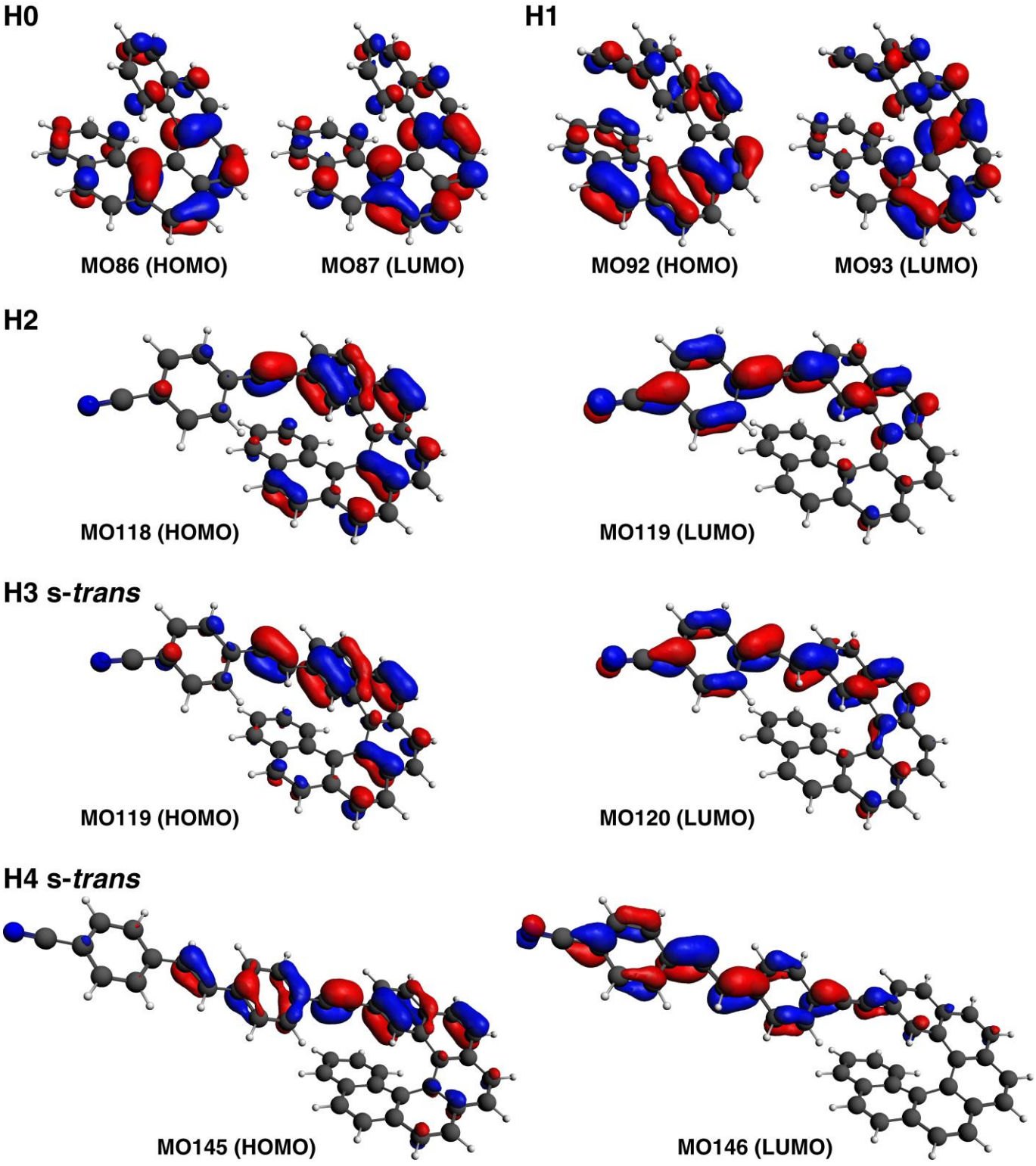

Fig. 11. HOMO and LUMO isosurfaces (0.04 au) of **H0**-**H4**. LC-PBE0/SV(P) calculations for MP2/cc-pVDZ (**H0**-**H3**) and BP-D2/DZ(P) (**H4**) structures.

LITTERATURE CITED

[1] Shen Y, Chen C-F. Helicenes: Synthesis and Applications. Chem Rev 2012;112:1463-1535.

[2] Martin RH. Helicenes. Angew Chem Int Ed 1974;13:649-659.

[3] Katz TJ. Syntheses of functionalized and aggregating helical conjugated molecules. Angew Chem Int Ed 2000;39:1921-1923.

[4] Urbano A. Recent developments in the synthesis of helicene-like molecules. Angew Chem Int Ed 2003;42: 3986-3989.

[5] Rajca A, MiyasakaM. in Functional Organic Materials (Eds.: Müller, T. J. J.; Bunz, U. H. F.), Wiley-VCH, Weinheim, 2007, pp. 543-577.

[6] Amabilino DB. Chirality at the Nanoscale: Nanoparticles, Surfaces, Materials and more: Wiley VCH; 2009.

[7] Gingras M. One hundred years of helicene chemistry. Part 3: applications and properties of carbohelicenes. Chem Soc Rev 2013;42:1051-95.

[8] Newman MS, Lednicer D. The synthesis and resolution of hexahelicene. J Am Chem Soc 1956;78: 4765-4770.

[9] Gingras M. One hundred years of helicene chemistry. Part 1: non-stereoselective syntheses of carbohelicenes. Chem Soc Rev 2013;42:968-1006.

[10] Bossi A, Licandro E, Maiorana S, Rigamonti C, Righetto S, Stephenson GR, Spassova M, Botek E, Champagne B. Theoretical and Experimental Investigation of Electric Field Induced Second Harmonic Generation in Tetrathia[7]helicenes. J Phys Chem C 2008;112:7900-7907.

[11] Mallory FB, Wood CS, Gordon JT. Photochemistry of stilbenes. III Some aspects of the mechanism of photocyclization to phenanthrenes. J Am Chem Soc 1964;86:3094-3102.

[12] Jorgensen KB. Photochemical oxidative cyclisation of stilbenes and stilbenoids-the Mallory-reaction. Molecules 2010;15:4334-4358

[13] Gingras M, Félix G, Peresutti R. One hundred years of helicene chemistry. Part 2: stereoselective syntheses and chiral separations of carbohelicenes. Chem Soc Rev 2013;42:1007-1050.

[14] Srebro M, Govind N, de Jong WA, Autschbach J. Optical Rotation Calculated with Time-Dependent Density Functional Theory: The OR45 Benchmark. J Phys Chem A 2011;115:10930-10949.

[15] Furche F, Ahlrichs R, Wachsmann C, Weber E, Sobanski A, Vögtle F, Grimme S. Circular dichroism of helicenes investigated by time-dependent density functional theory. J Am Chem Soc 2000;122:1717-1724.

[16] Grimme S, Harren J, Sobanski A, Vögtle F. Structure/Chiroptics relationships of planar chiral and helical molecules. Eur J Org Chem 1998;8:1491-1509.

[17] Botek E, Champagne BJ. Circular dichroism of helical structures using semiempirical methods. J Chem Phys 2007;127:204101/1-9.

[18] Graule S, Rudolph M, Vanthuyne N, Autschbach J, Roussel C, Crassous J, Réau R. Metal-bis(helicene) assemblies incorporating π-conjugated phosphole-azahelicene ligands: impacting chiroptical properties by metal variation. J Am Chem Soc 2009;131:3183-3185.

[19] Graule S, Rudolph M, Shen W, Lescop C, Williams JAG, Autschbach J, Crassous J, Réau R. Assembly of π-conjugated phosphole-azahelicene derivatives into chiral coordination complexes: a combined experimental and theoretical study. Chem Eur J 2010;16:5976-6005.

[20] Norel L, Rudolph M, Vanthuyne N, Williams JAG, Lescop C, Roussel C, Autschbach J, Crassous J, Réau R. Metallahelicenes: a novel family of easily accessible helicene derivatives exhibiting important and tuneable chiroptical properties. Angew Chem Int Ed 2010;49: 99-102.

[21] Anger E, Rudolph M, Norel L, Zrig S, Shen C, Vanthuyne N, Toupet L, Williams JAG, Roussel C, Autschbach J, Crassous J, Réau R. Multifunctional and reactive enantiopure organometallic helicenes: tuning chiroptical properties by structural variations of mono- and bis-(platinahelicene)s. Chem Eur J 2011;17:14178-14198.

[22] Anger E, Rudolph M, Shen C, Vanthuyne N, Toupet L, Roussel C, Autschbach J, Crassous J, Réau R. From hetero- to homo-chiral bis(metallahelicenes) based on a Pt^{III}-Pt^{III} bonded scaffold: isomerisation, structure and chiroptical properties. J Am Chem Soc 2011;133:3800-3803.

[23] Nakai Y, Mori T, Inoue Y. Circular Dichroism of (Di)methyl- and Diaza[6]helicenes. A Combined Theoretical and Experimental Study. Journal of Physical Chemistry A 2013;117:83-93.

[24] Nakai Y, Mori T, Inoue Y. Theoretical and experimental studies on circular dichroism of carbo[n]helicenes. J Phys Chem A 2012;116:7372-7385.

[25] Anger E, Srebro M, Vanthuyne N, Toupet L, Rigaut S, Roussel C, Autschbach J, Crassous J, Réau R. Ruthenium-vinylhelicenes: remote metal-based tuning and redox switching of the chiroptical properties of a helicene core. J Am Chem Soc 2012;134:15628-15631.

[26] Lightner DA, Hefelfinger DT, Powers TW, Frank GW, Trueblood KN. Hexahelicene - Absolute configuration. J Am Chem Soc 1972;94:3492-3497.

[27] Yao Y, Shen W, Nohra B, Lescop C, Réau, R. Coordination-driven Hierarchical Organization of π-Conjugated Systems: from Molecular to Supramolecular π-stacked Assemblies. Chem Eur J 2010; 16:7143-7163.

[28] Vanest JM, Gorsane M, Libert V, Pecher J, Martin RH. Helicenes. Photochemical ring-closure of polymer-supported 1,2-diarylethylenes. Hexahelicene- and benzo[c]phenanthrene-2-carboxaldehyde. Chimia 1975;29:343-4.

[29] Weigang OE Jr., Turner JA, Trouard PA. Emission polarization and circular dichroism of hexahelicene. J Chem Phys 1966;45:1126-1134.

[30] *TURBOMOLE V5.7.1 2005, Quantum Chemistry Group, University of Karlsruhe, Germany*.

[31] Ahlrichs R, Bär M, Häser M, Horn H, Kölmel C. Electronic structure calculations on workstation computers: The program system turbomole. Chem Phys Lett 1989;162:165-169.

[32] Becke AD. Density-functional exchange-energy approximation with correct asymptotic behavior. Phys Rev A 1988;38:3098-3100.

[33] Perdew JP. Density-functional approximation for the correlation energy of the inhomogeneous electron gas. Phys Rev B 1986;33:8822-8824.

[34] Perdew JP. Erratum: Density-functional approximation for the correlation energy of the inhomogeneous electron gas. Phys Rev B 1986;34:7406.

[35] Schäfer A, Horn H, Ahlrichs R. Fully optimized contracted Gaussian basis sets for atoms Li to Kr. J Chem Phys 1992;97:2571-2577.

[36] Eichkorn K, Weigend F, Treutler O, Ahlrichs R. Auxiliary basis sets for main row atoms and transition metals and their use to approximate Coulomb potentials. Theor Chem Acc 1997;97:119-124.

[37] Weigend F, Ahlrichs R. Balanced basis sets of split valence, triple zeta valence and quadruple zeta valence quality for H to Rn: Design and assessment of accuracy. Phys Chem Chem Phys 2005;7:3297-3305.

[38] Grimme S, Antony J, Ehrlich S, Krieg H. A consistent and accurate ab initio parametrization of density functional dispersion correction (DFT-D) for the 94 elements H-Pu. J Chem Phys 2010; 132:154104-154119.

[39] *ADF2012, SCM, Theoretical Chemistry, Vrije Universiteit, Amsterdam, The Netherlands*.

[40] Guerra CF, Snijders JG, te Velde G, E. J. Baerends EJ. Towards an order-N DFT method. Theor Chem Acc 1998;99:391-403.

[41] te Velde G, Bickelhaupt FM, Baerends EJ, Guerra CF, van Gisbergen SJA, Snijders JG, Ziegler T. Chemistry with ADF. J Comput Chem 2001;22:931-967.

[42] Gaussian 09, Revision A.02, Frisch MJ, Trucks GW, Schlegel HB, Scuseria GE, Robb MA, Cheeseman JR, Scalmani G, Barone V, Mennucci B, Petersson GA, Nakatsuji H, Caricato M, Li X, Hratchian HP, Izmaylov AF, Bloino J, Zheng G, Sonnenberg JL, Hada M, Ehara M, Toyota K, Fukuda R, Hasegawa J, Ishida M, Nakajima T, Honda Y, Kitao O, Nakai H, Vreven T, Montgomery Jr JA, Peralta JE, Ogliaro F, Bearpark M, Heyd JJ, Brothers E, Kudin KN, Staroverov VN, Kobayashi R, Normand J, Raghavachari K, Rendell A, Burant JC, Iyengar SS, Tomasi J, Cossi M, Rega N, Millam JM, Klene M, Knox JE, Cross JB, Bakken V, Adamo C, Jaramillo J, Gomperts R, Stratmann RE, Yazyev O, Austin AJ, Cammi R, Pomelli C, Ochterski JW, Martin RL, Morokuma K, Zakrzewski VG, Voth GA, Salvador P,

Dannenberg JJ, Dapprich S, Daniels AD, Farkas Ö, Foresman JB, Ortiz JV, Cioslowski J, Fox DJ. Gaussian, Inc., Wallingford CT, 2009.

[43] Dunning TH. Gaussian basis sets for use in correlated molecular calculations. I. The atoms boron through neon and hydrogen. J Chem Phys 1989;90:1007-1023.

[44] Bylaska EJ, de Jong WA, Govind N, Kowalski K, Straatsma TP, Valiev M, van Dam JJ, Wang D, Apra E, Windus TL, Hammond J, Autschbach J, Aquino F, Nichols P, Hirata S, Hackler MT, Zhao Y, Fan P-D, Harrison RJ, Dupuis M, Smith DMA, Glaesemann K, Nieplocha J, Tipparaju V, Krishnan M, Vazquez-Mayagoitia A, Jensen L, Swart M, Wu Q, Van Voorhis T, Auer AA, Nooijen M, Crosby LD, Brown E, Cisneros G, Fann GI, Fruchtl H, Garza J, Hirao K, Kendall R, Nichols JA, Tsemekhman K, Wolinski K, Anchell J, Bernholdt D, Borowski P, Clark T, Clerc D, Dachsel H, Deegan M, Dyall K, Elwood D, Glendening E, Gutowski M, Hess A, Jaffe J, Johnson B, Ju J, Kobayashi R, Kutteh R, Lin Z, Littlefield R, Long X, Meng B, Nakajima T, Niu S, Pollack L, Rosing M, Sandrone G, Stave M, Taylor H, Thomas G, van Lenthe J, Wong A, Zhang Z. NWChem, A Computational Chemistry Package for Parallel Computers, Version 6.1; Pacific Northwest National Laboratory, Richland, Washington 99352-0999, USA.; 2011.

[45] Valiev M, Bylaska E, Govind N, Kowalski K, Straatsma T, Dam HV, Wang D, Nieplocha J, Apra E, Windus T, de Jong W. NWChem: A comprehensive and scalable open-source solution for large scale molecular simulations. Comput Phys Commun 2010;181:1477-1489.

[46] Autschbach J. Time dependent density functional theory for calculating origin independent optical rotation and rotatory strength tensors. ChemPhysChem 2011;12:3224-3235.

[47] Autschbach J. Introduction to the computation of chiroptical properties with first-principles theoretical methods: Background and illustrative examples. Chirality 2009;21:E116-E152.

[48] McWeeny R. Methods of molecular quantum mechanics. Academic Press, London, 1992.

[49] Hansen AE, Bouman TD. Natural chiroptical spectroscopy: theory and computations. Adv Chem Phys 1980; 44: 545-644.

[50] Pedersen TB, Koch H, Boman L, de Merás AMJS. Origin invariant calculation of optical rotation without recourse to London orbitals. Chem Phys Lett 2004;393:319-326.

[51] Bak KD, Hansen AE, Ruud K, Helgaker T, Olsen J, Jørgensen P. Ab initio calculation of electric circular dichroism for trans-cyclooctene using London atomic orbitals. Theor Chim Acta 1995; 90:441-458.

[52] Krykunov M, Autschbach J. Calculation of optical rotation with time-periodic magnetic field-dependent basis functions in approximate time-dependent density functional theory. J Chem Phys 2005;123:114103(1)-114103(10).

[53] Kendall RA, Dunning TH, Harrison RJ. Electron affinities of the first-row atoms revisited. Systematic basis sets and wave functions. J Chem Phys 1992;96:6796-6806.

[54] Becke AD. Density-functional thermochemistry. III. The role of exact exchange. J Chem Phys 1993;98:5648-5652.

[55] Lee C, Yang W, Parr RG. Development of the Colle-Salvetti correlation-energy formula into a functional of the electron density. Phys Rev B 1988;37:785-789.

[56] Stephens PJ, Devlin FJ, Chabalowski CF, Frisch MJ. Ab Initio Calculation of Vibrational Absorption and Circular Dichroism Spectra Using Density Functional Force Fields. J Phys Chem 1994;98:11623-11627.

[57] Becke AD. A new mixing of Hartree–Fock and local density-functional theories. J Chem Phys 1993;98:1372-1377.

[58] Ernzerhof M, Scuseria GE. Assessment of the Perdew–Burke–Ernzerhof exchange-correlation functional. J Chem Phys 1999;110:5029-5036.

[59] Adamo C, Barone V. Toward reliable density functional methods without adjustable parameters: The PBE0 model. J Chem Phys 1999;110:6158-6170.

[60] Rohrdanz MA, Herbert JM. Simultaneous benchmarking of ground- and excited-state properties with long-range-corrected density functional theory. J Chem Phys 2008;129:034107(1)-034107(9).

[61] Srebro M, Autschbach J. Tuned Range-Separated Time-Dependent Density Functional Theory Applied to Optical Rotation. J Chem Theory Comput 2012;8:245-256.

[62] Newman MS, Lutz WB, Lednicer D. A New Reagent for Resolution by Complex Formation; The Resolution of Phenanthro-[3,4-c]Phenanthrene. J Am Chem Soc 1955;77: 3420-3421.

[63] Mort BC, Autschbach J. Magnitude of zero-point vibrational corrections to the optical rotation in rigid organic molecules: A time-dependent density functional study. J Phys Chem A 2005;109:8617-8623.

[64] Nohra B, Graule S, Lescop C, Réau R. Mimicking [2,2]Paracyclophane Topology: Molecular Clips for the Coordination-Driven Co-facial Assembly of π-Conjugated Systems. J Am Chem Soc 2006;128:3520-3521.

[65] Aranda Perez A. I, Biet T, Graule S, Agou T, Lescop C, Branda N. R, Crassous J, Réau R. Chiral and extended π-conjugated bis(2-pyridyl)phospholes as assembling N,P,N-pincers for the coordination-driven synthesis of supramolecular [2,2]paracyclophane analogs. Chem Eur J 2011;17: 1337-1351.

[66] Agou T, Sebastian M, Lescop C, Réau R. Folding of a supramolecular framework based on a tetrametallic clips driven by π–π interactions. Inorg Chem 2011;50:3183-3185.

[67] Vreshch V, Shen W, Nohra B, Yip S-K, Yam V.W-W, Lescop C, Réau, R. Aurophilicity versus mercurophilicity : impact of d^{10}-d^{10} metallophilic interactions on the structure of metal-rich supramolecular assemblies. Chem Eur J 2012;18:466-477.